7504 *Macromolecules* **2009**, *42*, 7504–7517
DOI: 10.1021/ma900533s

Macromolecules
ARTICLE

Self-Consistent Modeling of Constraint Release in a Single-Chain Mean-Field Slip-Link Model

Renat N. Khaliullin and Jay D. Schieber*

Center for molecular study of condensed soft matter and Department of Chemical and Biological Engineering, Illinois Institute of Technology, 3440 South Dearborn Street, Chicago, Illinois 60616

Received March 11, 2009; Revised Manuscript Received July 29, 2009

ABSTRACT: A new implementation of constraint dynamics for the discrete slip-link model (DSM), which is statistically consistent with sliding dynamics of the chain, is proposed. The DSM agrees with linear viscoelastic (LVE) data for linear monodisperse entangled polymer melts at least as well as state-of-the-art tube models. The agreement with data can be obtained by fitting only two parameters, β and τ_K that are independent of the molecular weight of the polymer. However, because the theory exists on a more-detailed level of description, it contains fewer assumptions than do existing tube models and assumptions of the latter may be examined. Several fundamental differences between DSM and tube models are revealed. For example, Rouse motion is an inappropriate realization of constraint dynamics in the slip-link picture. Moreover, the chain relaxation by sliding dynamics for the DSM is significantly different from the fraction of survived entanglements multiplied by the plateau modulus, whereas the tube model assumes that these are equivalent at long times. These two differences effectively cancel one another. Moreover, they could result in different bidisperse LVE predictions. On the other hand, several other assumptions made in tube theories are confirmed by the DSM results. Finally, model comparisons with experimental data exposed some limitations in the experiments.

Introduction

From the literature, one might expect the prediction of linear viscoelasticity for linear entangled polymers to be a solved problem. Several existing tube models show very good agreement with monodisperse linear-chain LVE data.[1−3] Although the models are self-consistent and data agreement is good, the tube models for linear systems cannot be generalized to branched systems or cross-linked networks without fundamental modifications. In addition, most existing tube models lack agreement with small-amplitude oscillatory shear flow experiments of bidisperse linear melts.

Experiments show that the relaxation modulus of bidisperse linear melts is not simply a superposition of the relaxation modulus of two monodisperse components. In other words, the relaxation of the environment has an important impact on the relaxation of a single chain. De Gennes[4] was the first to analyze the relaxation of the environment for a single-chain mean-field model, an effect called "constraint release". Later, Graessley implemented constraint release as a single-mode diffusive process based on "Rouse motion" in a tube model.[5] For simplification he made four assumptions:

1. As in prior tube models, the chain is assumed to be surrounded by a tube with equally spaced entanglements. These assumptions imply that the tension is constant along the chain and that the relaxation modulus of the chain $G(t)$ is equal to the fraction of the survived tube $\mu(t)$ times the plateau modulus G_N^0.
2. The chain sliding dynamics (SD) within the tube is represented as a 1-D diffusive process of the center of mass of the chain along the tube, called "reptation". The primitive-path length of the tube is held constant.
3. Constraint release is a single-mode diffusive process, where the tube is allowed to move as a Rouse bead−spring chain. Each bead fluctuates with the same mobility. Note that this assumption implies fluctuations in the primitive-path length, which may be inconsistent with the second assumption.
4. The total relaxation modulus is a product of relaxation by reptation and relaxation by constraint release, a so-called "factorization assumption". The assumption was added for mathematical simplification and has not been tested.

Graessley's model neglected contour-length fluctuations (CLF), which were found to improve the tube model significantly.[6] To account for relaxations faster than the reptation time, Rubinstein and Colby added CLF to Graessley's model.[1] In addition, they showed that single-mode Rouse motion of the tube segments gives poor agreement with experiments. They improved the model by introducing a spectrum of mobilities for the tube segments obtained consistently with CLF and reptation. However, CLF, reptation and Rouse motion processes were assumed to act independently.

Hua and Schieber incorporated constraint release for a slip-tube model by pairing entanglements on different chains in a simulation ensemble.[2] They modeled the chain as a Rouse bead−spring chain in a tube, which yields both reptation and CLF simultaneously. However, their implementation of constraint release violated detailed balance.

Doi and Takimoto also included constraint release by coupling the entanglements on different chains.[7] Whenever one chain destroyed or created an entanglement by SD, the coupled entanglement on another randomly chosen chain was destroyed or created by constraint release. This implementation improved detailed balance over that of Hua and Schieber. Nonetheless, in

*Corresponding authors. E-mail: schieber@iit.edu.

 Published on Web 09/11/2009

the Doi and Takimoto implementation, CLF was accounted for in a crude way, and detailed balance was still not rigorous.

In 2006, Nair and Schieber tested the approach to constraint release as Rouse motion on a slip-link model.[8] The slip-link model allowed them to avoid several assumptions made in tube models, such as constant entanglement spacing. Moreover, the relaxation modulus was not assumed to be proportional to the fraction of survived entanglements $f(t)$, or primitive-path fraction $\mu(t)$. $G(t)$ was calculated rigorously from the chain contribution to stress, avoiding the factorization assumption. Furthermore, reptation, CLF and constraint release were not assumed to be independent processes. The continuous spectrum of mobilities was calculated in a self-consistent way. However, despite having fewer assumptions, their results still showed worse agreement with data than that of Colby and Rubinstein. They observed that adding Rouse motion of the entanglements negatively impacted the agreement with experiments for monodisperse linear polymers compared to the slip-link model without constraint release. This observation suggests that implementation of constraint release as a Rouse motion is inappropriate for the slip-link model.

In this work, we avoid all four of Graessley's assumptions by using a discrete mean-field slip-link model. Our goal is to mimic constraint release on a mean-field chain in a self-consistent way, but avoiding coupling of entanglements on different chains à la Doi and Takimoto. This approach has several advantages over coupling. First, most (if not all) stochastic models require numerical solution, meaning that either an ensemble of independent chains, or a single chain for long times is simulated. Coupling entanglements on different chains prevents taking advantage of computational parallelization. Second, it is not necessary to assume that entanglements are binary interactions. Third, using our implementation, we can study the separate contributions of chain dynamics with and without constraint release. Our results will show that the slip-link model agrees with both data and the theoretical predictions of des Cloizeaux[9] and of Likhtman and McLeish[3] for monodisperse systems. However, further analysis shows that the individual contributions from SD and constraint release are very different from what is seen in tube formulations. In other words, there are significant conceptual differences between the models.

We will show first, that the relaxation spectrum $G(t)$ is not proportional to primitive-path survival, and second, constraint release is not described by Rouse motion. Those differences suggest that our prediction for the linear viscoelasticity of linear polydisperse entangled melts should differ significantly from the one made by the Likhtman and McLeish model, for example. In addition, future work will show that use of the slip-link theory instead of the tube theory allows us to create a unified mathematical model that can be applied to linear entangled polydisperse polymers and branched systems without significant modifications either physically or mathematically.

The Discrete Slip-Link Model

Equilibrium Statistics. The slip-link concept was introduced by Doi and Edwards[10] in 1978 to motivate use of a certain equation in their tube model, and it was later more fully developed by Schieber et al.[8,11,12] In 2003, Schieber introduced the discrete slip-link model (DSM) that is significantly evolved in the present work.

In the slip-link model, the chain is assumed to be well described as a random walk, which we expect to hold for polymeric chains with contour length and entanglement spacing longer then several Kuhn steps. The chain has a constant number of Kuhn segments N_K, where each Kuhn segment has constant length a_K. The random walk of N Kuhn steps between two entanglements of separation Q can

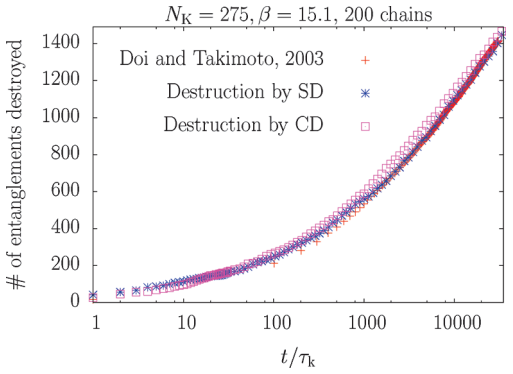

Figure 1. Number of entanglements destroyed over time by the two processes: CD (⊡) and SD (∗). The results are compared to the Doi and Takimoto entanglement-pairing algorithm (+).

be approximated by a Gaussian free energy

$$\frac{F_s(\boldsymbol{Q}, N)}{k_B T} = \frac{3Q^2}{2Na_K^2} + \frac{3}{2}\ln\left[\frac{2\pi N a_K^2}{3}\right] \quad (1)$$

where k_B is the Boltzmann constant and T is temperature. For the equilibrium dynamics considered here, where chains are not stretched by flow, the Gaussian free energy is expected to hold. The free energy of the dangling ends can be calculated from the probability distribution of the entangled strand. After integrating the distribution over all possible positions of one entanglement, the free energy of the dangling ends turn out to be a constant, which we set to zero. The free energy of the entire chain is a sum of free energies of entangled strands

$$F(\Omega) = \sum_{i=2}^{Z-1} F_s(\boldsymbol{Q}_i, N_i) \quad (2)$$

where Z is the number of strands, N_i is the number of Kuhn steps in the i^{th} strand, and $\boldsymbol{Q}_i$ is the orientation vector between entanglement $i-1$ and $i+1$.

In this work, we use a DSM,[11] meaning that the number of Kuhn steps shifted from one strand to another is an integer. The Kuhn step shuffling between neighboring strands is driven by Brownian forces and free energy differences. The advantage of the DSM over the continuous version is a rigorous destruction and creation of the entanglements at chain ends. In the discrete version, the entanglement is destroyed when a dangling end is abandoned by the last Kuhn step. The creation process is fully determined from detailed balance. On the other hand, in the continuous implementation of the theory, creation and destruction are managed by defining a nonzero free energy of the dangling ends.[8]

In this work, we also introduce a new implementation of constraint release. Since the constraints are not just destroyed, but also added in the middle of the entangled chain, we call the process "constraint dynamics" (CD).

Before explaining the details, we point out that this implementation reproduces the main idea of the Doi and Takimoto algorithm[7] in Figure 1. This figure compares the number of entanglements of independent chains destroyed in time by CD and by SD. Only initially created entanglements are considered. The destruction obtained from two processes is identical within the noise introduced by the limited ensemble size. We recreated the Doi and Takimoto pairing algorithm for stronger comparison (while avoiding the other limitations). Thus, when one entanglement was destroyed by

SD the other was destroyed automatically. The agreement of the three curves in Figure 1 illustrates that our implementation can mimic the Doi and Takimoto algorithm well without actually pairing different chains in the ensemble.

In order to mimic the process of spontaneous destruction and creation of entanglements on a chain without pairing different ensemble members, each entanglement on the chain is assigned a characteristic lifetime τ^{CD} upon its creation. This variable characterizes the time necessary for the imaginary paired chain to destroy the entanglement by SD, causing destruction of the entanglement on the probed chain. As a result, the conformation variables have been changed from that before[8,11,13] to be $\Omega \equiv (Z, \{N_i\}, \{\boldsymbol{Q}_i\}, \{\tau_i^{CD}\})$. Where τ_i^{CD} is the characteristic lifetime of entanglement i related to CD. The number of entanglements on a chain is fluctuating, so the environment behaves as an entanglement "bath". The modified Maxwell−Boltzmann relation for such a chain is

$$p_{eq}(\Omega) = \frac{\delta(N_K, \sum_{i=1}^{Z} N_i)}{J} \exp\left[-\frac{F(\Omega)}{k_B T}\right] \times \exp\left[\frac{\mu^E(Z-1)}{k_B T}\right] \prod_{i=1}^{Z-1} p^{CD}(\tau_i^{CD}) \quad (3)$$

where $\delta(i,j) := \delta_{i,j}$ is the Kronecker delta function, J is a normalization constant, and $p^{CD}(\tau_i^{CD})$ is a probability density for the ith entanglement to have a characteristic CD lifetime τ_i^{CD}. The Kronecker delta function is responsible for the conservation of Kuhn steps in a chain. The second exponential in eq 3, which includes the entanglement chemical potential of the surroundings, μ^E, takes care of fluctuations in the number of entanglements on the chain. Note that presence of CD does not affect equilibrium $\{\boldsymbol{Q}_i\}$ and $\{N_i\}$ distributions, which are determined by the free-energy. It is convenient to define

$$\beta := \exp\left(-\frac{\mu^E}{k_B T}\right) \quad (4)$$

as a model parameter that depends on polymer chemistry and solvent concentration and assumed to be independent of temperature. This temperature-independence assumption fails if the chain flexibility changes significantly; however we neglect this possible dependence here.

Equilibrium Dynamics. As a result of discretizing the number of Kuhn steps in a strand, the evolution equation at equilibrium has the form

$$\frac{\partial p_{eq}(\Omega, t|\Omega_0, t_0)}{\partial t} = \int [W(\Omega|\Omega') p_{eq}(\Omega', t|\Omega_0, t_0) - W(\Omega'|\Omega) p_{eq}(\Omega, t|\Omega_0, t_0)]\, d\Omega' \quad (5)$$

where $W(\Omega'|\Omega)$ is a transition probability of a jump from conformation Ω to conformation Ω' per unit time. The transition probability can be separated into several parts

$$W = \left(\sum_{i=1}^{Z-1} W_{sh}^i\right) + W_d^{SD} + W_c^{SD} + W_d^{CD} + W_c^{CD} \quad (6)$$

where W_{sh}^i represents Kuhn-step shuffling, W_d^{SD} and W_c^{SD} represent destruction and creation of the entanglements on the ends of the chain due to SD, and finally W_d^{CD} and W_c^{CD} represent destruction and creation of the entanglements in the middle of the chain due to CD. The transition probability to shift a Kuhn step between strands i and $i+1$ is

$$W_{sh}^i(\Omega'|\Omega) = \delta_{Z,Z'} \prod_{j=2}^{Z-1} \delta(\boldsymbol{Q}_j - \boldsymbol{Q}_j') \prod_{j=1}^{Z-1} \delta(\tau_j^{CD} - \tau_j^{CD'}) \times \prod_{j=1, j\neq i, i+1}^{Z} \delta_{N_j, N_j'} (\delta_{N_i, N'_i - 1} \delta_{N_{i+1}, N'_{i+1}+1} + \delta_{N_i, N'_i+1} \delta_{N_{i+1}, N'_{i+1}-1}) \frac{2(\beta+1)}{\tau_K (N_i + N_{i+1})} \exp\left[\frac{F(\Omega') - F(\Omega)}{2 k_B T}\right] \quad (7)$$

The first line in the equation preserves conformations of the strands that are not involved in the Kuhn step shuffling through entanglement i. The second line ensures that only one Kuhn step can be shuffled at a time through entanglement i. The last line shows that Kuhn step shuffling is a result of Brownian forces as well as free energy differences. τ_K is a time constant related to the friction coefficient of a single step in the chain, which depends only on the chemistry and temperature of the polymer (and solvent concentration, if present). In the present work, the total chain friction is assumed to be proportional to the number of Kuhn steps in the entire chain. Hence, the total friction of the chain is constant.[8] The fraction in the last line is the result of constant chain friction. In addition, the transition probability satisfies detailed balance (section 6 in ref 14).

For convenience, we combine all the delta functions that preserve conformation of a single strand into the shorthand

$$\delta_{\Omega_i, \Omega'_k} := \delta_{N_i, N'_k} \delta(\tau_i^{CD} - \tau_k^{CD'}) \delta(\boldsymbol{Q}_i - \boldsymbol{Q}_k') \quad (8)$$

In order to manage creation and destruction by SD, we use a simple form for the destruction rate, which depends only on the friction of the Kuhn segment. As a result, the creation transition probability calculated from detailed balance yields a Gaussian distribution for the newly entangled strand. We present the solution for one chain end, where the other end solutions $W_{c,Z}^{SD}(\Omega'|\Omega)$ and $W_{d,Z-1}^{SD}(\Omega'|\Omega)$ are similar and reported in the Appendix

$$W_d^{SD}(\Omega'|\Omega) = \delta_{Z,Z'+1} \delta_{N_2, N'_1 - 1} \delta_{N_1, 1} \frac{2(\beta+1)}{\tau_K (N_2+1)} \prod_{j=2}^{Z} \delta_{\Omega_j, \Omega'_{j-1}} + W_{d,Z-1}^{SD}(\Omega'|\Omega),$$

$$W_{c-1}^{SD}(\Omega'|\Omega) = \delta_{Z,Z'-1} \delta_{N_1, N'_2+1} \times H(N_1 - 2) \frac{2(\beta+1) p^{CD}(\tau_1^{CD'})}{\tau_K \beta N_1} \times \left[\frac{3}{2\pi(N_1-1)a_K^2}\right]^{3/2} \times \exp\left[-\frac{3\boldsymbol{Q}_2'^2}{2(N_1-1)a_K^2}\right] \prod_{j=2}^{Z} \delta_{\Omega_j, \Omega'_{j+1}} + W_{c,Z}^{SD}(\Omega'|\Omega) \quad (9)$$

The first Kronecker delta function in each line of eq 9 manages the change in the number of strands; the second ensures that only one Kuhn step is involved in the destruction and creation process. The third delta function for $W_d^{SD}(\Omega'|\Omega)$ and Heaviside step function, $H(x)$, for $W_c^{SD}(\Omega'|\Omega)$ allow destruction to occur when there is only one Kuhn step left in a dangling end; otherwise, creation is allowed. If we integrate $W_c^{SD}(\Omega'|\Omega)$ over all possible

conformations Ω', we obtain the probability of creating an entanglement for a chain with conformation Ω

$$w_c^{SD}(\Omega) = \frac{2(\beta+1)}{\tau_K \beta}\left[\frac{H(N_1-2)}{N_1}+\frac{H(N_Z-2)}{N_Z}\right] \quad (10)$$

The constraint dynamics destruction transition probability for the i^{th} entanglement is handled like a first-order reaction

$$W_d^{CD}(\Omega'|\Omega) = W_{d,1}^{CD}(\Omega'|\Omega)+\sum_{i=2}^{Z-2} W_{d,i}^{CD}(\Omega'|\Omega) + W_{d,Z-1}^{CD}(\Omega'|\Omega) \quad (11)$$

We write it in this way, because the end strands require slightly different notation. The first end is written as

$$W_{d,1}^{CD}(\Omega'|\Omega) = \delta_{Z,Z'+1}\frac{1}{\tau_1^{CD}}\prod_{j=3}^{Z}\delta_{\Omega_j,\Omega'_{j-1}}\delta(\boldsymbol{Q}_1')\delta_{N_1+N_2,N'_1} \quad (12)$$

The Dirac delta function kills the entangled strand near the end, and the Kronecker deltas preserve the proper number of Kuhn steps.

$$W_{d,i}^{CD}(\Omega'|\Omega) = \delta_{Z,Z'+1}\frac{1}{\tau_i^{CD}}\prod_{j=1}^{i-1}\delta_{\Omega_j,\Omega'_j}\prod_{j=i+2}^{Z}\delta_{\Omega_j,\Omega'_{j-1}} \times \delta(\boldsymbol{Q}_i+\boldsymbol{Q}_{i+1}-\boldsymbol{Q}_1')\delta_{N_i+N_{i+1},N'_i} \quad (13)$$

where the delta functions in the second line preserve the location and total number of Kuhn steps in the neighboring strands involved in the destruction process.

From detailed balance we get the transition probability to create an entanglement by CD

$$W_c^{CD}(\Omega'|\Omega) = W_{c,1}^{CD}(\Omega'|\Omega)+\sum_{i=2}^{Z-1} W_{c,i}^{CD}(\Omega'|\Omega)+W_{c,Z}^{CD}(\Omega'|\Omega) \quad (14)$$

For the first strand, the transition probability is

$$W_{c,1}^{CD}(\Omega'|\Omega) = \delta_{Z,Z'-1}\prod_{j=2}^{Z}\delta_{\Omega_j,\Omega'_{j+1}}\delta_{N_1,N'_1+N'_2}H(N_1-2) \times \frac{p^{CD}(\tau_1^{CD'})}{\tau_1^{CD'}\beta}\left[\frac{3}{2\pi N'_2}\right]^{3/2}\exp\left[-\frac{3\boldsymbol{Q}_2'^2}{2N'_2}\right] \quad (15)$$

Expressions of transition probabilities of creation and destruction of the last entanglement are given in the Appendix, and the intermediate steps have

$$W_{c,i}^{CD}(\Omega'|\Omega) = \delta_{Z,Z'-1}\prod_{j=1}^{i-1}\delta_{\Omega_j,\Omega'_j}\prod_{j=i+1}^{Z}\delta_{\Omega_j,\Omega'_{j+1}}H(N_1-2) \times\delta(\boldsymbol{Q}_i-\boldsymbol{Q}_i'-\boldsymbol{Q}_{i+1}')\delta_{N_i,N'_i+N'_{i+1}}\frac{p^{CD}(\tau_i^{CD'})}{\tau_i^{CD'}\beta} \times\left[\frac{3}{2\pi N'_i\left(1-\frac{N'_i}{N_i}\right)}\right]^{3/2}\exp\left[-\frac{3\left(\boldsymbol{Q}_i'-\frac{N'_i}{N_i}\boldsymbol{Q}_i\right)^2}{2N'_i\left(1-\frac{N'_i}{N_i}\right)}\right] \quad (16)$$

After integrating over all possible conformations Ω', we get the probability to create an entanglement anywhere on the chain

$$w_c^{CD}(Z) = \frac{(N_K-Z)}{\beta}\int_0^\infty \frac{p^{CD}(\tau^{CD})}{\tau^{CD}}\,d\tau^{CD} \quad (17)$$

Note that from eq 17 the probability to create an entanglement along the chain is uniform, which also agrees with the physical picture.

From eqs 10 and 14 it is clear that SD creates entanglements with the characteristic lifetime τ^{CD} with probability density $p^{CD}(\tau^{CD})$; however, CD creates entanglements with probability density $p^{CD}(\tau^{CD})/(\tau^{CD})$, which weights the short-lived entanglements greater than long-lived ones, i.e. short-lived entanglements will be destroyed more often than long-lived ones, so they must be created more frequently in order to satisfy the equilibrium statistics given by $p^{CD}(\tau^{CD})$. Most predictions of the theory must be found numerically, so mathematical details on the simulation procedure are given in the Appendix.

Determination of Constraint Dynamics Parameters. In this section we show how to construct $p^{CD}(\tau^{CD})$ self-consistently. We assume binary events for entanglements, although the model is not restricted to that number of interacting chains. In order to check CD we need to compare it with SD: destruction by both processes should be equal in time. This comparison was made in Figure 1.

First, we follow the fraction of survived entanglements, $f(t)$, as a function of time when no CD is present. Similar to what was shown in previous works[1,3] for tube segments, the lifetime distribution $p^{CD}(\tau^{CD})$ is related to $f(t)$ by

$$f(t) = \int_0^\infty p^{CD}(\tau^{CD})\exp\left(-\frac{t}{\tau^{CD}}\right)d\tau^{CD} \quad (18)$$

However, for eq 14 it is necessary to find $p^{CD}(\tau^{CD})/(\tau^{CD})$, which is related to the time derivative of the fraction of survived entanglements

$$f_d(t) := \frac{\dot{f}(t)}{\dot{f}(0)} = \frac{\int_0^\infty \frac{p^{CD}(\tau^{CD})}{\tau^{CD}}\exp\left(-\frac{t}{\tau^{CD}}\right)d\tau^{CD}}{\int_0^\infty \frac{p^{CD}(\tau^{CD})}{\tau^{CD}}\,d\tau^{CD}} \quad (19)$$

As has been mentioned by Likhtman and McLeish,[3] $f_d(t)$ has more interesting features that might be lost by simply looking at $f(t)$. If we follow the survival time of entanglements from an arbitrary point in time, we estimate $f(t)$; however, it is more efficient to follow the cumulative distribution of the survival time of entanglements from their individual time of creation, which is equal to $1-f_d(t)$.

From Figure 2 and Figure 3 it appears that $f_d(t)$ has a slightly curved power-law region, followed by a single exponential. The single exponential term is likely a result of reptation-like motion, and the power-law is CLF. Even though reptation and CLF are not specified in the model as separate processes, we clearly observe them as parts of SD relaxation. This result could be taken as confirmation of the assumptions made by Rubinstein and Colby,[1] who treat these processes separately. The slightly curved power-law region can be obtained from the derivative of a stretched exponential

$$\frac{d}{dt}\exp\left[-\left(\frac{t}{\tau_0}\right)^\alpha\right] = -\alpha\left(\frac{t}{\tau_0}\right)^{\alpha-1}\exp\left[-\left(\frac{t}{\tau_0}\right)^\alpha\right] \quad (20)$$

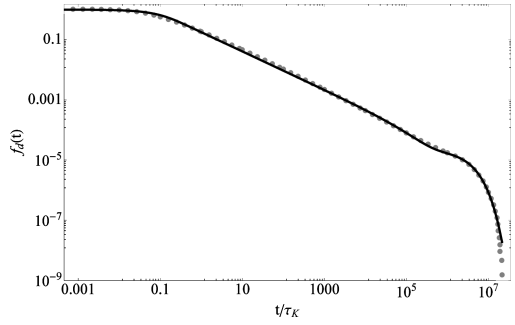

Figure 2. Fraction of survived entanglements $f_d(t)$ on log−log scale from 50 chains simulation for $10^8\tau_K$ each with $N_K = 922, \beta = 15.1$. The solid line is eq 23 with parameters given in the second line of Table 1.

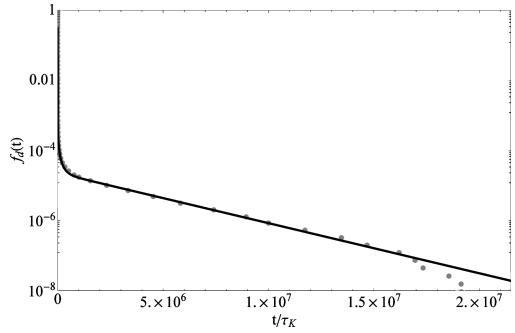

Figure 3. Same results as in Figure 2, but on a semilog plot to illustrate the single exponential.

which means that $f(t)$ is a combined curve of both stretched and single exponentials. The relaxation spectrum of the stretched exponent can be approximated with a power-law,[15] while the single exponential is a delta function. Therefore, we assume the following form for the normalized lifetime distribution probability

$$p^{\mathrm{CD}}(\tau) = \frac{(1-g)\alpha}{(\tau_{\max}^{\alpha}-\tau_0^{\alpha})}\tau^{\alpha-1}H(\tau-\tau_0)H(\tau_{\max}-\tau)+g\delta(\tau_{\mathrm{d}}-\tau) \tag{21}$$

where g, α, τ_0, $\tau_{\max}$, and τ_{d} are constants. We find that this form fits simulation results for chains of arbitrary β,N_K and τ_K very well. Inserting eq 21 into eq (18), $f(t)$ becomes

$$f(t) = \frac{(1-g)\alpha\left[\Gamma\left(-\alpha, \frac{t}{\tau_{\max}}\right)-\Gamma\left(-\alpha, \frac{t}{\tau_0}\right)\right]t^{\alpha}}{\tau_{\max}^{\alpha}-\tau_0^{\alpha}} + g\,\exp\left(-\frac{t}{\tau_{\mathrm{d}}}\right) \tag{22}$$

where $\Gamma(a,b)$ is the incomplete gamma function. We obtain the continuous curves shown in Figures 2−4 by fitting the parameters g, α, τ_0, $\tau_{\max}$, and τ_{d} to the simulation results. The fitting was performed by the least-squares method of relative residuals. The residuals between the fit and simulations are smaller than 5%. Note the remarkable simplicity, and the presence of only five parameters (g, α, τ_0, $\tau_{\max}$, τ_{d}). Although, the parameters are determined from a best fit, they are not considered adjustable parameters of the model; they are determined in a self-consistent way with the model, which has only two parameters, N_K and β.

Equation 22 has a form similar to that proposed by Likhtman and McLeish[3] for the fraction of survived tube

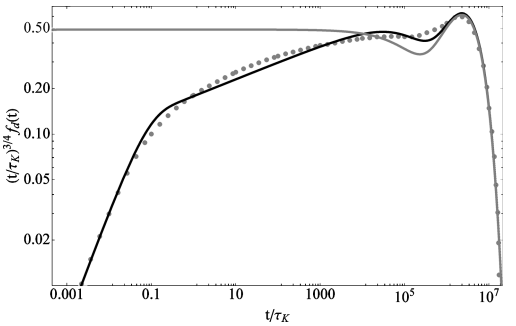

Figure 4. Same results as Figure 2, plotted the way suggested in reference[3] to express differences between simulation results and fit. Gray continuous line is renormalized $-\tau_e^{1/4}t^{3/4}\partial u(t)/\partial t$ predicted by Likhtman and McLeish assuming $\tau_e = 6.7\tau_K$.

$\mu(t)$ of a 1D Rouse chain in a tube if we set

$$g^{\mathrm{LM}} = \frac{8(1-1.69/\sqrt{Z}+2.0/Z-1.24/Z^{3/2})}{\pi^2},$$

$$\alpha^{\mathrm{LM}} = 1/4, \quad \tau_0^{\mathrm{LM}} = 0, \quad \tau_{\max}^{\mathrm{LM}} = \tau_e Z^4\left(\frac{1-g}{4\times0.306}\right)^4,$$

$$\tau_{\mathrm{d}}^{\mathrm{LM}} = 3\tau_e Z^3(1-2\times1.69/\sqrt{Z}+4.17/Z-1.55/Z^{3/2})$$

For the tube model, τ_e is an adjustable time constant comparable to, but somewhat larger than τ_K. However, we find that α is approximately 1/3 for the DSM, and slightly dependent on N_K and β (see Table 1 and Figure 4). The comparison of our model prediction for $f(t)$ with the Likhtman and McLeish $\mu(t)$ for polystyrene 500 kDa is illustrated in Figure 5. Even though the exponents of the power-law are not the same and g is somewhat different, the difference between $f(t)$ and $\mu(t)$ is very small. Nonetheless, our results clearly show an exponent different from $^1/_4$. The difference of DSM predictions with CLF, from those of 1D Rouse motion in a tube could be related to a finite length effect between entanglements that slows down CLF. Note that the 1D Rouse chain is a phantom chain, so that the ends can easily pass through each other, completely obliterating the tube. As shown in Table 1, α values decrease with molecular weight of a chain. If we extrapolate α dependence toward very long chains we find $\alpha = 1/4$ for chains with $M_w \sim 100$ MDa for PS.

The fitted parameters for eq 21 used in several systems considered in this paper are shown in Table 1.

After the CD parameters are determined from the fitting, we compare destruction by SD to CD when CD is present. Our simulations have shown that when CD is added, the SD reptation time τ_{d} always decreases roughly by 10%, resulting in faster relaxation than without CD. From the comparison we determine new CD parameters by iteration until destruction by SD and CD are equal within the error introduced by the ensemble size as shown in Figure 1. However, the relaxation modulus obtained using the iterated CD spectrum has negligible difference from the one calculated using the first guess; this means that iterations for the CD spectrum are not essential for monodisperse linear chains. That is why the values for parameters in Table 1 are not found by iteration. However, the CD influence on SD could be significantly different for bidisperse and branched systems and could explain the "dynamic tube dilution" physics[16] required to fix tube model predictions for branched systems.

Analysis of Relaxation Modulus Predictions. The stress tensor $\boldsymbol{\tau}(t)$ of the model is determined by thermodynamics

Table 1. Parameters Set for Calculation of $p^{CD}(\tau^{CD})$ Using Eq 21 and $\beta = 15.1$ without iterations. Also given for comparison are Values for the Comparable Parameters in the Likhtman−McLeish Tube Model[a]

N_K	α	τ_0/τ_K	τ_{max}/τ_K	g	τ_d/τ_K	g^{LM}	τ_{max}^{LM}/τ_K	τ_d^{LM}/τ_K
83	0.42 ± 0.02	0.06 ± 0.01	$(5 \pm 2) \times 10^2$	0.60 ± 0.05	1720 ± 30	0.45	783	1511
220	0.40 ± 0.01	0.06 ± 0.01	$(6 \pm 2) \times 10^3$	0.65 ± 0.04	$33 \pm 1 \times 10^3$	0.55	14×10^3	37×10^3
244	0.40 ± 0.01	0.06 ± 0.01	$(9 \pm 2) \times 10^3$	0.63 ± 0.06	$47 \pm 1 \times 10^3$	0.55	20×10^3	52×10^3
489	0.38 ± 0.01	0.07 ± 0.01	$(4 \pm 1) \times 10^4$	0.68 ± 0.03	$31 \pm 8 \times 10^4$	0.61	18×10^4	50×10^4
922	0.36 ± 0.01	0.08 ± 0.01	$(3 \pm 1) \times 10^5$	0.69 ± 0.02	$31 \pm 3 \times 10^5$	0.66	15×10^5	39×10^5

[a] For high-molecular-weight polystyrene, we find that $\tau_e \cong 10.5\tau_K$, which is assumed throughout this table.

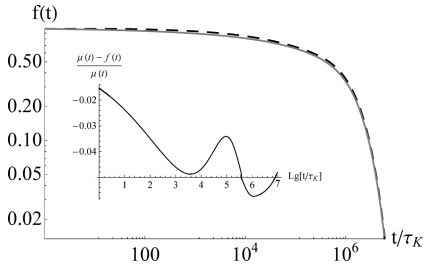

Figure 5. Fraction of survived entanglements for PS 500 kDa in the DSM $f(t)$ (dashed black line) and the Likhtman and McLeish prediction $\mu(t)$,[3] eq 13 (gray line). The inset is the relative residuals.

to be[8,11]

$$\tau(t) = -n\left\langle \sum_{j=2}^{Z-1} \boldsymbol{Q}_j \left(\frac{\partial F(\Omega)}{\partial \boldsymbol{Q}_j} \right)_{T,\{N_j\},\{\boldsymbol{Q}_{i\neq j}\}} \right\rangle \tag{23}$$

where n is the number density of polymer chains, and $\langle ... \rangle$ is an ensemble average. The relaxation modulus $G(t)$ can be found using the Green−Kubo expression

$$G(t) = \frac{1}{nk_BT}\langle \tau_{xy}(0)\tau_{xy}(t)\rangle_{eq} \tag{24}$$

However, experimental data are usually presented in the frequency domain $G^*(\omega) := i\omega\mathcal{F}[G(t)]$, where

$$\mathcal{F}[...] := \int_0^\infty ... \, e^{-i\omega t} \, dt$$

is a half-sided Fourier transform, because small-amplitude oscillatory shear flow experiments are much easier to perform compared to step strain relaxation experiments. In order to weight such information equally To calculate the Fourier transform of our results, we fit the simulated relaxation modulus, sampled equally on a logarithmic scale, with a continuous curve, from which we take the analytical Fourier transform. Mathematically the problem is solved by finding the continuous spectrum of relaxation times, $h(\tau)$, that gives us the same relaxation modulus

$$G(t) = G_N^0 \int_0^\infty \frac{h(\tau)}{\tau} \exp\left(-\frac{t}{\tau}\right) d\tau \tag{25}$$

As in the experimental data, we find that the power-law spectrum proposed by Baumgaertel, Schausberger, and Winter[17] describes our simulation results well

$$h(\tau) = \frac{\sum_{i=1}^{m} \tau^{\alpha_i} H(\tau_i - \tau) H(\tau - \tau_{i-1}) \prod_{j=1}^{i-1} \tau_j^{\alpha_j - \alpha_{j+1}}}{\sum_{i=1}^{m} \frac{\tau_i^{\alpha_i} - \tau_{i-1}^{\alpha_i}}{\alpha_i} \prod_{j=1}^{i-1} \tau_j^{\alpha_j - \alpha_{j+1}}} \tag{26}$$

where m is the number of modes in the spectrum, τ_i and α_i are corresponding time constants and power-law exponents, respectively. The complex modulus, G^*, is calculated from the Fourier transform of the relaxation modulus multiplied by $i\omega$, using $\{\alpha_i, \tau_i\}$ as fitting parameters

$$G'(\omega) = G_N^0\omega^2 \sum_{i=1}^{m} \frac{\prod_{j=0}^{i-1} \tau_j^{\alpha_j - \alpha_{j+1}}}{\alpha_i + 2} \times \left[{}_2F_1\left(1, \frac{\alpha_i+2}{2}; \frac{\alpha_i+4}{2}; -\omega^2\tau_i^2\right)\tau_i^{\alpha_i+2} - {}_2F_1\left(1, \frac{\alpha_i+2}{2}; \frac{\alpha_i+4}{2}; -\omega^2\tau_{i-1}^2\right)\tau_{i-1}^{\alpha_i+2} \right] \Big/ \sum_{i=1}^{m} \frac{\prod_{j=0}^{i-1} \tau_j^{\alpha_j - \alpha_{j+1}} (\tau_i^{\alpha_i} - \tau_{i-1}^{\alpha_i})}{\alpha_i} \tag{27}$$

$$G''(\omega) = G_N^0\omega \sum_{i=1}^{m} \frac{\prod_{j=0}^{i-1} \tau_j^{\alpha_j - \alpha_{j+1}}}{\alpha_i + 1} \times \left[{}_2F_1\left(1, \frac{\alpha_i+1}{2}; \frac{\alpha_i+3}{2}; -\omega^2\tau_i^2\right)\tau_i^{\alpha_i+1} - {}_2F_1\left(1, \frac{\alpha_i+1}{2}; \frac{\alpha_i+3}{2}; -\omega^2\tau_{i-1}^2\right)\tau_{i-1}^{\alpha_i+1} \right] \Big/ \sum_{i=1}^{m} \frac{\prod_{j=0}^{i-1} \tau_j^{\alpha_j - \alpha_{j+1}} (\tau_i^{\alpha_i} - \tau_{i-1}^{\alpha_i})}{\alpha_i} \tag{28}$$

where ${}_2F_1(a,b;c;z)$ is the hypergeometric function.

From eqs 23 and 24 one can calculate the plateau modulus[11]

$$G_N^0 = G(0) = nk_BT\langle (Z-2)H(Z-2)\rangle_{eq} = \frac{\rho RT}{M_w}\left[\left(\frac{\beta}{\beta+1}\right)^{N_K-1} + \frac{N_K - \beta - 2}{\beta+1} \right] \tag{29}$$

Note that

$$\lim_{N_K \to \infty} G_N^0 = \frac{\rho RT}{M_K(\beta+1)} \tag{30}$$

where M_K is the molecular weight of a Kuhn step, M_w is the molecular weight of the polymer chain, ρ is polymer density, and R is the ideal gas constant.

Note that the theoretical plateau modulus G_N^0 (eq 29) is larger than the apparent plateau modulus seen in $G^*(\omega)$ experiments. The former is reached at frequencies where glassy dynamics begin to dominate the measurements, which are not included in the model.

Theoretical Predictions

Comparison with Polystyrene Data. We compare here our predictions to experimental data; in the following, we compare

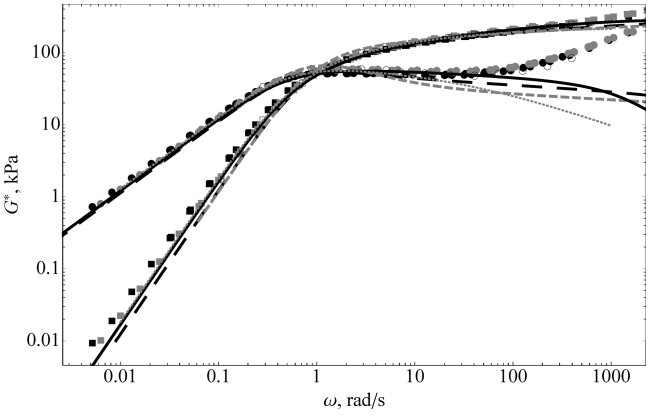

Figure 6. G data for polystyrene with M_w = 200 kDa at 170. Experimental data are indicated with squares and circles for G' and G'' respectively: open black (○) PS200B,[20] filled black PS200N,[21] gray (●) PS200S.[22] Theoretical predictions with N_K = 275 and β = 15.1(G_N^0 = 280 kPa) are also shown. The black long-dashed line is the DSM prediction with CD and τ_K = 50 μs, the gray short-dashed line is the DSM without CD and τ_K = 16 μs, the dotted gray line is the prediction made by the des Cloizeaux model, the solid black line is the prediction of the Likhtman and McLeish model using an approximation for the constraint-release contribution $R(t)$ to the relaxation modulus as $\mu^{1.2}$.

the DSM with tube model results. The DSM requires three input parameters: $N_K = M_w/M_K$, β, and τ_K. The second parameter is estimated from the plateau modulus of the polymer using eq 30, and τ_K, is fitted to a single LVE experiment.

For polystyrene M_K = 720 Da[18] and β is estimated to be 15.1, with corresponding plateau modulus G_N^0 = 280 kPa. The model prediction for a polystyrene melt with M_w = 200 kDa with and without CD is presented in Figure 6. From the figure we see that inclusion of CD (black dashed line) not only decreases the relaxation time by a factor of 3, but improves the shape significantly. We see that the presence of CD affects the shape of the G'' curve. The observed narrowing of the peak width when CD (gray dashed lines) is switched off is consistent with what is observed experimentally by Liu et al. for short probe chains in a matrix of very long chains.[19]

In addition, a slight scatter is observed in the experimental data in Figure 6, related to variations in the observed plateau modulus. We observed that variations from lab to lab in the apparent plateau can be as high as 20%. All oscillatory measurements are performed in plate−plate geometry and we assume that the variations in these measurements are related to the very strong dependence on the radius of the sample (e.g., the apparent modulus ~ radius^4). So we allow slight shifts of the experimental data in the modulus value by multiplying the measured G' and G'' by a shift factor b. The values of the shift factor b are given in Table 2. For the plateau modulus we do not observe any systematic trend in the shift factor, so we assume that deviations are experimental uncertainties. Unfortunately, these uncertainties in the sample radius make an accurate estimation of β difficult. Fortunately, the shape of $G(t)$ is not strongly sensitive to the exact value of β. The time dependence of the model prediction is normalized by the time constant τ_K, which can be determined from fitting simulation results to a single experimental data set. The adjustment of the time constant does not influence the shape of the relaxation modulus, but shifts it in the frequency domain.

In order to use a single value of τ_K for all molecular weights, we find that the data should be taken in the same lab for two reasons; first, even though temperature control may be good,

Table 2. Experimental Data Characteristics, and Parameter Fits[a]

code	$10^{-3}M_w$	M_w/M_n	T,°C	N_K	τ_K,ms	B	source
PS39	39	1.07	143	54	5	1	26
PS60	60	1.04	170	83	0.1	1	27
PS102	102	1.02	130	140	36	1	25
PS160	160	N/A	160	220	0.18	1.25	24
PS177	177	1.03	170	244	0.1	1	27
PS200B	200	1.04	130	275	36	1	20
PS200N	200	1.06	150	275	0.16	1	21
PS200S	200	1.06	175	275	0.05	1	22
PS355	355	1.02	170	489	0.05	1	23
PS390	390	1.06	130	537	36	1	25
PS427	427	1.05	143	588	5	1.25	26
PS670	670	N/A	160	922	0.18	1.25	24
PBD44	44	1.04	28	191	9×10^{-5}	1	28

[a] Parameter b is a factor used to shift the data vertically that accounts for uncertainty in sample radius.

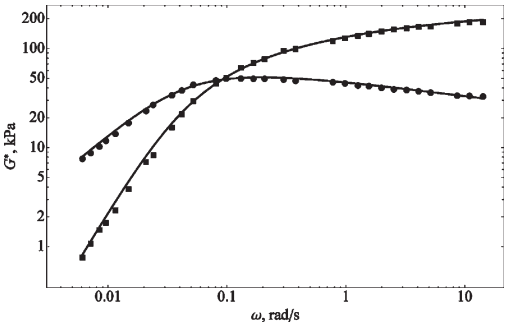

Figure 7. PS355[23] symbols are experimental data, and lines are the theoretical predictions.

the thermocouple calibration may vary by a few degrees. As a result of such variations, the time constant τ_K may change significantly (for PS, τ_K(130 °C) = 1.6 τ_K (132 °C)); second, remaining solvent, even down to a half percent, significantly decreases the relaxation time, causing additional variation in τ_K. The variations in the time domain are observed for the experimental data for polystyrene 200 kDa. The master curve shown in Figure 6 is obtained from the data reported by several laboratories for different temperatures by shifting them to the same temperature of 175 °C using the time-temperature superposition reported in ref 20.

Nonetheless, if the measurements are performed in the same lab, we fit the time constant using a theoretical prediction compared with experimental data for a single high-molecular-weight sample. No adjustment is performed for low-molecular-weight samples. Figure 7, Figure 8 and Figure 9 show excellent agreement with the data for PS102, PS160, PS355, and PS390 for several decades of frequency. The sample abbreviations are listed in Table 2. The deviation at high frequency is the glassy mode contribution, which is not considered in the model. For sample PS670 we can see a difference in shape between the prediction and experimental data. We observe that experimental G'' data in the plateau region near the crossover has a smaller slope than expected for samples with such a high molecular weight. We believe that this discrepancy might be a result of polydispersity of the sample. Unfortunately, the polydispersity index is not reported in ref 24. The fitted time constants are reported in Table 2.

τ_K is fitted to long-chain experimental data, so when looking at sufficiently low-molecular-weight systems, it would be necessary to change τ_K slightly to achieve a good fit. This trend can be seen in Figure 10 and Figure 11 for PS60 and PS39 respectively. It appears that the theory underpredicts the data only for PS samples with molecular weight

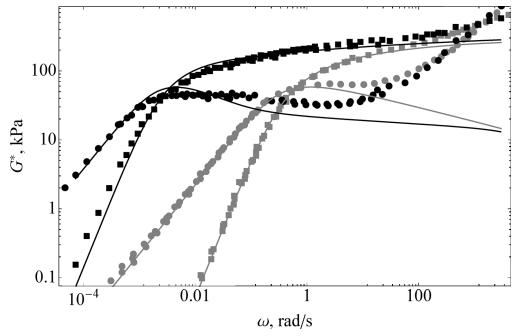

Figure 8. PS160 gray and PS670 black[24] symbols are experimental data and lines are the theoretical predictions.

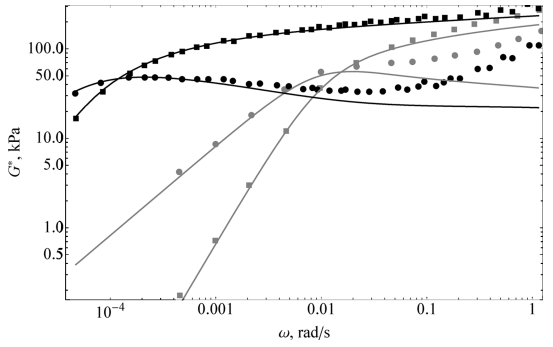

Figure 9. PS102 gray and PS390 black[25] symbols are experimental data and lines are the theoretical predictions.

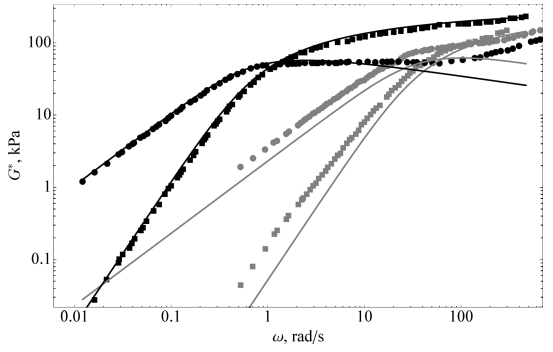

Figure 10. PS60 gray and PS177 black[27] symbols are experimental data and lines are the theoretical predictions.

less than approximately 100 kDa, or five entanglements. In Figure 12 we can clearly see that the model gives an accurate prediction of the scaling of the zero-shear-rate viscosity, η_0, with molecular weight. However, the experimental zero-shear-rate viscosity deviates from this scaling at small molecular weights as was also observed by Onogi et al.[29] The relaxation of the polymer is slower than predicted. We believe that the discrepancy might result from the coarse-graining utilized in the model. The model assumes that entangled strands can sample all possible conformation in a τ_K time. Furthermore, the relaxation in the model is solely determined by entanglements, and the deviation observed in Figure 12 for η_0 occurs for chains that have less than five entanglements on average. Another possible explanation for the discrepancy is discussed below.

In order to analyze the model performance without an arbitrary shift factor b or fitting τ_K, we can also use a Cole−Cole plot seen in Figure 13. This plot shows the

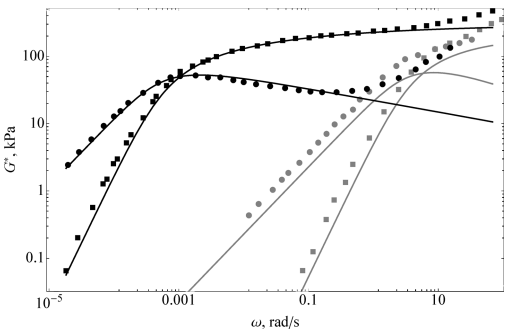

Figure 11. PS39 gray and PS427 black[26] symbols are experimental data and lines are the theoretical predictions.

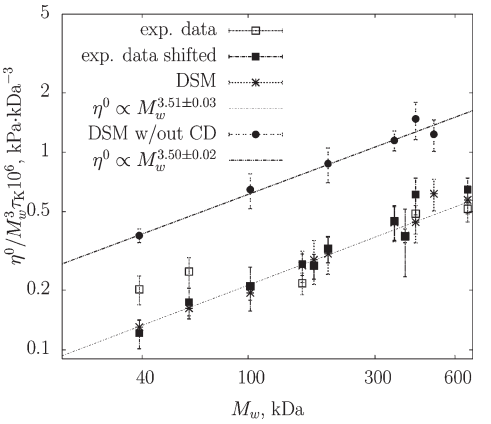

Figure 12. Zero-shear-rate viscosity scaling plot for polysyrene. η^0 values for experimental data were calculated from a data fit with a single-mode BSW (eq 26) assuming $\tau_0 = 0$. The shifts of experimental values are reported in 2. Additionally, values for PS39 and PS60 were shifted by 40% and 30% respectively corresponding to the shifts made in Figure 15.

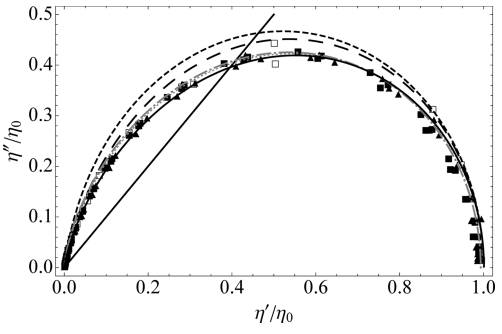

Figure 13. Cole−Cole plot for PS 200 kDa. Open black (□) PS200B,[20] black (■) PS200N,[21] black triangle (▲) PS200S.[22] Theoretical predictions with $N_K = 275$ and $\beta = 15.1 (G_N^0 = 280$ kPa) are also shown. The black long dashed line is the DSM prediction with CD, the black short dashed line is the DSM without CD, the gray dot-dashed line is the continuous slip-link with CD, the dotted gray line is the prediction made by the des Cloizeaux model, the solid black line is the prediction of the Likhtman and McLeish model. The solid straight black line helps one to locate the crossover point position.

correlation between the complex viscosities η' and η'', normalized with η_0, where $\eta^* = \eta' - i\eta'' := G^*/i\omega$. Renormalization by η_0 removes the sample radius dependence; second, the Cole−Cole plot depends parametrically on frequency, meaning that no τ_K fit is necessary. Figure 13 compares the PS 200 kDa data from Figure 6 with the theoretical prediction, alongside the tube model predictions of des Cloizeaux[9]

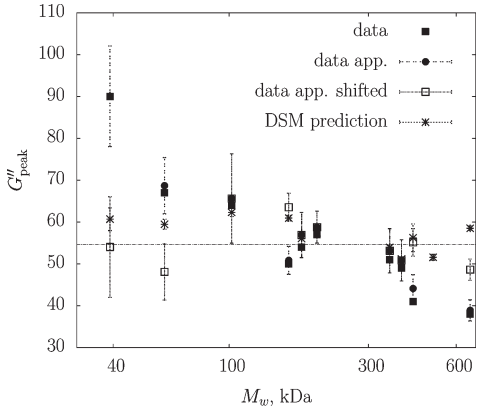

Figure 14. Local maximum of G'' for different molecular weight polystyrenes. Black squares (■) are maximum values of G'' that rigorously obtained from curve fitted by single mode BSW assuming $\tau_0 = 0$, black circles (●) are values obtained from $G''_{peak} \approx G^0_N[0.58\alpha/(0.37 + 1.15\alpha)]$. The line is a mean-square fit to the DSM predictions equal to 54.7 ± 0.7 kPa independent of molecular weight. The shifts for PS39 and PS60 are the same as in Figure 15, which agrees with the observations of Liu et al.[30] The remaining shifted data are for sample radius uncertainty, Table 2.

and of Likhtman and McLeish.[3] Here we see that all models result in very similar predictions.

Check with the Analysis of Liu et al. The plateau modulus is typically assumed to be the contributions from dynamics dominated by entanglements, as is the case for tube models and the slip-link model. However, as shown above, the predicted height of the plateau modulus can lie hidden in a frequency range dominated by glassy dynamics. Hence, the apparent plateau modulus extracted from data (e.g., at the minimum in the phase angle), always lies somewhat below the theoretical prediction, eq 30. However, Liu et al.[30] studied the molecular weight dependence of the local maximum G''_{peak} in the loss modulus that occurs near the crossover point for monodisperse systems. This quantity is observable experimentally, and predictable from models that contain only entanglement-dominated dynamics (and no glassy mode predictions). They found that the height of the peak was independent of molecular weight, whereas tube models and Likhtman's slip-spring simulation (SSS) predicted a height that increases with molecular weight. On the other hand Auhl et al. found a slight rise with molecular weight for G''_{peak} values for PS.[39]

In Figure 14 we show G''_{peak} predicted by the DSM together with G''_{peak} values obtained from the experimental data. Experimental values were calculated by fitting the BSW spectrum to the data and finding the maximum of the G'' curve. We find that experimental data can be described by a single-mode BSW spectrum (eq 26), and setting $\tau_0 = 0$; then G''_{peak} can be accurately approximated by $0.58\ \alpha\ G^0_N/(0.37 + 1.15\ \alpha)$. The comparison of the actual maximum of the fitted spectra and the values using this approximation are shown in Figure 14. The DSM predicts that G''_{peak} is independent of molecular weight, in agreement with ref 30, and on average equal to 54.7 ± 0.7 kPa for PS.

However, in contradiction with ref 30, the data used here show a decrease in the peak value with molecular weight. This dependence could be a result of increasing polydispersity with molecular weight, which would not contradict the observations of Liu et al. In particular, the peak disappears for unentangled chains, which makes the results for the two least-entangled systems puzzling. Figure 14 also shows experimental G''_{peak} values for higher molecular weights that

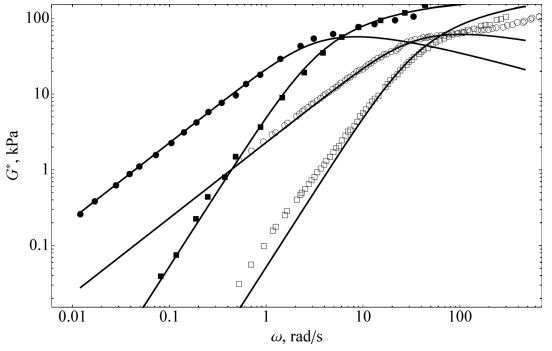

Figure 15. Experimental data for PS39[26] shifted by 40% (black) and for PS60[27] shifted by 30% (open black) with corresponding DSM predictions.

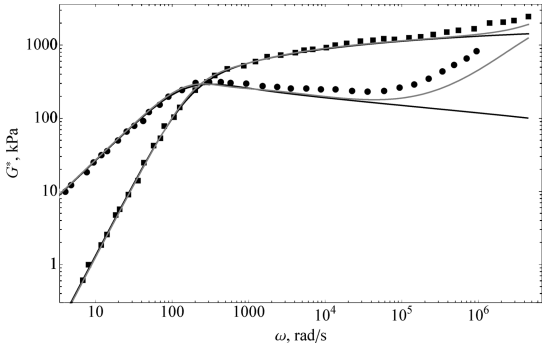

Figure 16. PBD44 black[28] symbols are experimental data and lines are the theoretical predictions by the DSM (black) and the Likhtman and McLeish model with glassy modes (gray). $\beta = 5.1$, which corresponds to $G^0_N = 1.74$ MPa and $M_e = 1.34$ kDa, and $\tau_K = 0.09\ \mu$s.

were vertically shifted by a shift factor b to account for sample radius uncertainty, reported in Table 2. Note that the direction of shift is toward aligning G''_{peak} values for the data as suggested in ref 30. If we also shift the two lower molecular weight samples, PS39 and PS60, to agree with the constant G''_{peak} values as suggested by ref 30, we find much closer agreement with theory, Figure 15. In other words, it is precisely the unexpected vertical shifts in data that lead to the discrepancy in G^* values.

Comparison with Polybutadiene and Universality. Finally, we compare the DSM predictions to monodisperse PBD data of 44 kDa[28] in Figure 16 and find good agreement. Note that Likhtman and McLeish also compared tube model predictions with the data shown in Figure 16, and concluded that there might not be universality for all entangled, monodisperse polymer melts. Their conclusions relied on two aspects of the tube theory that differ from the slip-link theory considered here. First, the tube theory predicts that the entanglement-dominated dynamics can be reduced to a function of the average number of entanglement strands $\langle Z \rangle_{eq}$ alone. All chemistry specific properties of the polymer are assumed to just rescale time (through the adjustable parameter τ_e), and volume through the entanglement density. Second, the tube model includes terms that are intended to describe the glassy modes. As mentioned above, the slip-link theory has coarse-grained out the glassy modes.

Note that the slip-link theory does *not* predict universality for entanglement-dominated dynamics. For instance, the plateau modulus (eq 29 depends not only on the fraction

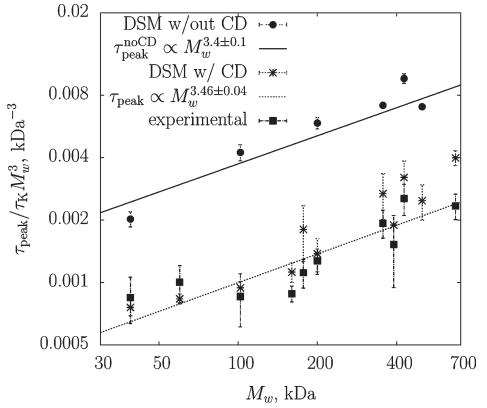

Figure 17. Time values that correspond to a maximum values of G''. The experimental values are obtained by fitting G^* measurements with a single mode BSW (eq 27) assuming $\tau_0 = 0$ and approximating $\tau_{peak} = \tau_{max}(\alpha(1.5 - 0.5\alpha))^{1/(1-\alpha)}$.

$N_K/(\beta + 1)$ (which is equivalent to tube prediction for $\langle Z \rangle_{eq}$), but also on the bare parameter β. We can rewrite our expression for the plateau modulus, eq 30 as

$$G_N^0 = \frac{\rho RT}{M_K(\beta+1)}\left\{1+\frac{\beta+1}{N_K}\left[\left(\frac{\beta}{\beta+1}\right)^{N_K-1} - 1 - \frac{1}{\beta+1}\right]\right\} \quad (31)$$

The prefactor $\rho RT/[M_K/(\beta + 1)]$ is the plateau modulus for an infinitely long, monodisperse system. The prefactor $(\beta + 1)/N_K$ inside the curly brackets is the universal part of the correction for finite length. However, the remaining bits cannot be reduced to a similar universal ratio.

It is not yet clear whether this lack of universality in entanglement dynamics might salvage the failure of universality between entanglement and glassy modes found for tube models. However, it does reopen the door for finding a connection between glassy modes and the parameters τ_K and β.

Examination of Tube Model Assumptions. In this section we examine some of the tube model assumptions mentioned previously. We compare our model to that presented by Likhtman and McLeish,[3] which we take as "state of the art" in monodisperse LVE tube-model calculations. The agreement between the discrete slip-link and Likhtman and McLeish models with experimental data is within experimental uncertainty as seen in Figure 6 and Figure 13. Since our model is on a sufficiently detailed level of description, we can examine each of the assumptions in the tube model for consistence with a slip-link picture. Finally, we also examine an assumption recently questioned by the analysis of Liu et al.[30] concerning the importance of constraint release on the scaling of the zero-shear-rate viscosity with molecular weight.

Assumption 1. The Total Relaxation Modulus Is a Product of Relaxation by SD and Relaxation by CD, the So-Called "Factorization Assumption". From eq 6 we see that by eliminating specific terms, we can turn off SD or CD. As shown in Figure 19, the product (■) of the relaxation modulus predicted with CD only (○) and the modulus predicted with SD only (□) lies within the error bars of the numerical calculation of the full relaxation modulus, which was obtained by simulating both dynamical processes simultaneously (●). Figure 19 shows that the factorization assumption does not introduce any significant error.

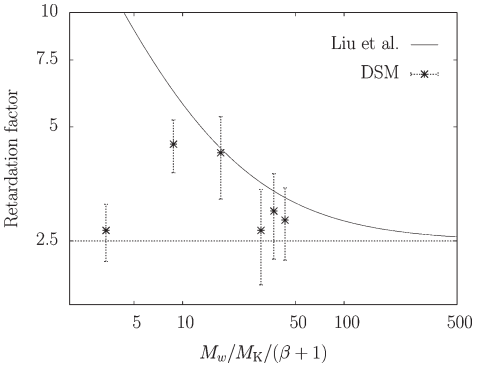

Figure 18. Retardation factor for PS. Continuous line is a prediction by Liu et al.[19] given by $R = 2.5(1 + 13(\beta + 1)M_K/M_w)$.

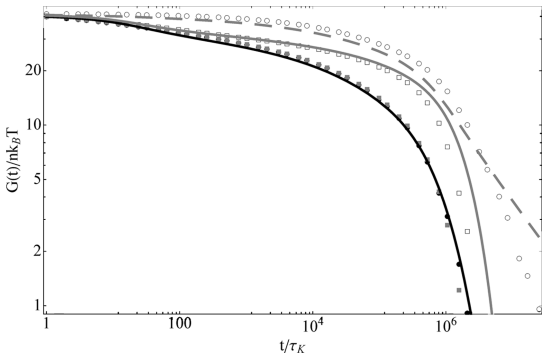

Figure 19. Relaxation modulus for PS 500 kDa. Empty circles are CD only, empty squares are SD only, black filled circles contain both processes and gray squares are a product of CD only with SD only. The continuous lines are the theoretical predictions by the Likhtman and McLeish[3] model. The continuous gray line is $^4/_5 G_N^0 \mu(t)$ + longitudinal modes, the dashed gray line is the relaxation modulus for CD managed with the Rouse motion and the black line is a product of two relaxation moduli.

Although, SD relaxation changes slightly when CD is present we do not observe any significant differences between the total relaxation curve when SD and CD are present and the factorized relaxation modulus.

Assumption 2. The Dynamics of the Chain in the Tube is Described by a 1D Rouse Chain. The main contribution to the chain relaxation comes from contour length fluctuations and reptation of the chain center of mass in a tube of fixed contour length. As was shown in the previous section, we observe separate CLF and reptation regions in the chain relaxation, even though we made no such assumptions about the chain dynamics. However, the exponent α in the power-law region of eq 21 is different from that calculated by Likhtman and McLeish from a 1D Rouse chain.

Assumption 3. The Relaxation Modulus without CD Is Approximated as the Product of the Fraction of Survived Tube and the Plateau Modulus plus Additive Contributions from Longitudinal Relaxation at Short Times. From Figure 19, it is clear that this assumption significantly overestimates the relaxation modulus for the slip-link model at long times. We point out that since tube models assume uniform entanglement spacing, the fraction of surviving entanglements is equivalent to the fraction of surviving tube. This equivalence is not true for the slip-link model. Therefore, one could also look at the fraction μ_{sl} of surviving primitive-path length in the slip-link model, and make a similar comparison. While there is a small difference (not shown) between $f(t)$ and $\mu_{sl}(t)$, the conclusion is the same: the relaxation modulus is not

proportional to either of these quantities. The difference between $G(t)$ and $\mu(t)$ could be studied by comparing DSM and tube models with dielectric relaxation experiments.[36,37]

Assumption 4. Constraint Dynamics Is a Diffusive Process of a Rouse Bead−Spring Chain That Represents the Surrounding Tube. In Figure 19, we also compare predictions by DSM and the Likhtman and McLeish tube model for relaxation moduli with CD only. The details of calculation of the Rouse relaxation modulus, $R(t)$, are given in the Appendix. The figure suggests that CD as a Rouse-like motion significantly underestimates the relaxation modulus predicted by the DSM with CD only at short times, and overestimates at long times. The source of this discrepancy was left unanswered in ref 31. We believe the discrepancy is related to the constant number and the constant mobility of entanglements in the Rouse approximations. The constraints cannot be removed by Rouse motion. However, in our implementation due to the CD process the number of entanglements on the chain fluctuates. Also, in the Rouse motion implementation, even though the mobility spectrum is continuous, when a bead is assigned one diffusion coefficient it keeps this value until it is killed by SD. In the slip-link CD implementation, when a short-lived entanglement is destroyed, there could be created a long-lived entanglement in its neighborhood.

In the DSM the relaxation by sliding dynamics is significantly faster than relaxation by constraint dynamics. However, in the tube models both relaxation curves are similar. When the two relaxation curves are multiplied, these differences nearly cancel each other, so the final relaxation curve agrees with the experimental results and our slip-link theory. These observations suggest that polydisperse predictions using the discrete slip-link theory and the Likhtman and McLeish theory could be rather different. We also expect a difference in branched chain predictions.

A few years after introduction of the slip-link theory,[11,12,32,33] Likhtman introduced a similar slip-spring simulation (SSS).[34] The simulation exists on a level of description that is even more detailed than the slip-link model, so can likewise be used to test tube model assumptions. However, there are a few differences between the two models utilizing slip-links: Likhtman's slip-links are elastic, instead of rigid; unlike DSM,[32] the SSS algorithm has not been analyzed for compliance with nonequilibrium thermodynamics; the SSS keeps track of the spatial positions of all monomers in the chain; the SSS contains two additional parameters related to the elasticity of the slip-links, and their mobility; there remains an open question about the proper inclusion of the slip-link elasticity in the stress tensor; and the number of entanglements in a simulations is handled in a microcanonical way for the simulation ensemble, rather than as a bath for the single chain.

Ramirez et al.[35] made comparisons between this simulation, and the tube model. They were unable to calculate the constraint release contributions to the relaxation modulus but instead took the ratio of the moduli with and without constraint release. The Fourier transform of this quantity was found to be well approximated by the primitive-path survival probability, in contradiction to our observations. The reasons for the different conclusions are not clear, but may be related either to the approximation used by them to estimate $R(t)$ for the SSS, to the less detailed comparisons made in that paper (as a result of the approximation necessary to estimate the contribution of constraint release), or to the difference in how sliding dynamics creates and destroys slip-links.

Assumption 5: The 3.5 Exponent for the Molecular Weight Scaling of the Zero-Shear-Rate Viscosity Is a Result of Reptation and Primitive-Path Length Fluctuations; Constraint Release Is Unimportant. Tube theories can switch off constraint release, or equivalently, slip-link theories can switch off constraint dynamics. Therefore, this is not strictly an assumption of tube theories, but was used in ref 38 to reconcile tube theory and experiment. More complete calculations have avoided it. However, one can examine the contribution of constraint dynamics only indirectly in experiments. To minimize this limitation, Liu et al. considered blends of extremely long chains with mildly to moderately entangled short chains. Consideration of bidisperse blends is outside the scope of this paper. However, those authors were able to clearly distinguish the time scales of short chains from those of long chains, and claimed to extract the dynamics of short chains with no constraint dynamics. They conclude that constraint dynamics (or release) has a significant impact on the molecular-weight scaling of the longest relaxation times.

Here we will perform a similar analysis for chains with no constraint dynamics. As a result, we find disagreement between theory and their results. However, we will argue that their analysis cannot remove the influence of constraint dynamics, nor the contribution of the long chains.

To estimate the longest relaxation time of a monodisperse system, Liu et al.[19] estimated the longest relaxation time as the peak time, $\tau_{peak} := 1/\omega_{peak}$, that corresponds to G''_{peak}. Second, they measure G^* for bidisperse blends of 80 mass % very long chains, and 20% by mass short chains. The loss modulus then shows two peaks, which are easily assigned to long and short chains. They examined the molecular-weight scaling of this time scale for the short chains in both monodisperse systems. They find two trends. First, the ratio of the times, $\tau_{peak}{}^{noCD}/\tau_{peak}$, (called the "retardation factor") is found to be greater than 2 for short chains, in contradiction with double reptation assumptions. Second, they find that τ_{peak} for the short chains in the blends scales with molecular weight to the 3.1 power. Hence, they conclude that short chains without significant constraint release nearly exhibits classic reptation scaling.

Here, we perform the same analysis for short chains with and without constraint dynamics. The retardation factor as a function of molecular weight as predicted by theory is shown in Figure 18. Liu et al. found that an empirical expression described their expressions reasonably well (note that the location of a maximum in data or simulations is difficult to determine with great accuracy). For all but the shortest chain, we find agreement with their predictions. We will argue that this is fortuitous below.

In Figure 17, we examine the scaling of τ_{peak} with and without constraint dynamics. We find that the scaling with constraint dynamics follows very well the scaling for η_0, giving an exponent of 3.46 ± 0.04, suggesting that the analysis of Liu et al. is reasonable. However, when constraint dynamics is switched off, the scaling exponent remains unchanged at 3.4 ± 1. The η_0 scaling is very similar, Figure 12.

We believe that the analysis of Liu et al. neglects the dynamics of the longer chains. Note that 20% of the entanglements on the longer chain are relaxing from constraint dynamics on the same time scale as the shorter chains. This relaxation contributes to the stress at roughly the same magnitude as the short-chain relaxation, and cannot be separated experimentally. Also, note that the constraint dynamics relaxation has a much longer tail than does sliding dynamics. Hence, these relaxation modes in the long chains—constraint dynamics of entanglement with short chains—will push the apparent relaxation time out to longer times. The analysis of Liu et al. would mistakenly assign

these relaxations to sliding dynamics of short chains alone. However, it should include an indirect effect of long chain constraint dynamics.

Less important, the long chain primitive-path fluctuations exist at all time scales, and account for approximately 40% of the long chain relaxation, estimated by extrapolating our slip-link results to long chains. Because this latter effect is continuous, the analysis of Liu et al. might effectively remove it.

Conclusions

We used the discrete slip-link model (DSM) with constant chain friction and self-consistent constraint dynamics (CD) to predict the linear viscoelasticity of linear monodisperse polymers. The model requires two fitting parameters: τ_K, related to the average time for a Kuhn step to jump through a given entanglement, and β related to the entanglement spacing on a chain. The N_K parameter is determined from the molecular weight of the chain. Recent atomistic simulations show that β can be estimated a priori.[13] Only τ_K is adjustable. The model chain exhibits primitive-path-length fluctuations and chain stretching, so it can also be applied to flows.

The new implementation of CD significantly improves the linear viscoelastic predictions. The comparisons of linear viscoelastic predictions of monodisperse polystyrene with experimental data showed good agreement at all frequencies except in the glassy region. This discrepancy of the model with experimental data at high frequencies is related to the coarse-grained level of description. The model agrees with experiments within uncertainty. For more precise comparison, it would be necessary to improve experimental accuracy, such as: sample radius control, thermocouple calibration between different laboratories, and complete solvent removal. The discrepancies related to the experimental control can be seen in Figure 6, where in addition to time-temperature superposition shifts, in order for the other data to agree with Schweizer et al., we must shift the Bach et al. data by a factor of 0.65 and the Nair et al. data by a factor of 0.13 in the frequency domain.

We tested several basic assumptions made in tube models. It appears that three assumptions are reasonable: (*i*) factorization of the relaxation modulus into sliding dynamics and constraint dynamics, (*ii*) separation of primitive path survival into reptation and CLF, and (*iii*) constraint dynamics does not influence molecular-weight scaling of the longest relaxation time.

However, the approximation of the relaxation modulus by the fraction of survived tube at long times, and approximation of CD by Rouse-like motion of the entanglements introduce fundamental differences with the slip-link model. After multiplying the CD and SD relaxation moduli for tube models, the differences cancel each other providing good agreement between tube and slip-link models. Additionally, we observed that the presence of CD slightly influences SD relaxation. These differences are expected to be more pronounced for polydisperse and branched systems.

The model predicts the correct zero-shear-rate viscosity scaling with molecular weight ($M_w^{3.51}$) for polystyrene.[29] However, experimental data for short chains deviate slightly from this power-law when the average number of entanglements $\langle Z\rangle_{eq} - 1$ is less than 5. This discrepancy of the model with experimental data for short chains is also likely due to the coarse-grained level of description. Liu et al.[30] observed that the height of the peak in the loss modulus was independent of molecular weight, which agrees with slip-link predictions, but is not in accord with tube model predictions. On the other hand, we disagree with the analysis of bidisperse blends by these authors. Alternatively,we did note that the height of the peak in G'' for the data considered here did not agree with observations made in,[30] or with expected trends. If the data were "corrected" to agree with these observations, good agreement was found with theory, even for these lightly entangled chains.

Finally, the agreement between the discrete version of the slip-link theory, and the continuous one showed that the continuous-model implementation of destruction and creation processes is reasonable.

Acknowledgment. Support of this work by the National Science Foundation under Grant No. NSF-SCI 05063059 and Army Research Office Grant W911NF-08-2-0058 are gratefully acknowledged.

Appendix

Equilibrium Distribution Probabilities. In this section, we point out a correction to the calculations of equilibrium distributions for the DSM mentioned in a previous work.[11] The equilibrium statistics is fully defined by the free energy, so CD does not affect it.

In order to test our numerical code using equilibrium statistics we need to obtain the equilibrium distribution of the number of strands, $P_{eq}(Z)$, the distribution of the number of Kuhn steps in the strands, $P_{eq}(N)$, and the probability density of the distances between entanglements, $p_{eq}(Q)$, of a chain. $P_{eq}(Z)$ is reported in eq A3 in ref 11. $P_{eq}(N)$ is calculated as follows:

$$\begin{aligned} P_{eq}(N) &= \sum_{Z=1}^{N_K}\sum_{i=1}^{Z} P_{eq}(Z,N_i)\delta(N_i - N) \\ &= \frac{\left(\frac{\beta}{\beta+1}\right)^N (N_K - N + 2\beta + 1)}{\beta(N_K+\beta)} H(N_K - N - 1) \\ &\quad + \left(\frac{\beta+1}{N_K+\beta}\right)\left(\frac{\beta}{\beta+1}\right)^{N_K-1}\delta_{N_K N} \end{aligned} \tag{32}$$

where $P_{eq}(Z,N_i)$ is given in eq A4 in ref 11. Equation 32 is different from eq A5 of ref 11, which is valid only for long chains.

Unfortunately, the distribution $p_{eq}(Q)$ cannot be calculated analytically. However, it may be found numerically from

$$p_{eq}(Q) = \sum_{N=1}^{N_K} p_{eq}(Q|N) P_{eq}(N) \tag{33}$$

where $p_{eq}(Q|N)$ is reported in ref 12, and $P_{eq}(N)$ is given by eq 32.

Numerical Algorithm for the Slip-Link Model. Here we derive the Gillespie algorithm for numerical solution of the model. Similar to Brownian dynamics, we simulate trajectories and average over ensembles. Our algorithm is first order, such that the chain conformation Ω changes only by one Kuhn step per Δt. As a result Δt is a function of Ω. Further we show how the calculation of the Δt is performed.

We start by integrating eq 5 from the beginning of the time step t_0 to the end $t_0 + \Delta t$

$$\begin{aligned} &p_{eq}(\Omega, t_0+\Delta t|\Omega_0, t_0) - \delta(\Omega - \Omega_0) \\ &= \int \left[W(\Omega|\Omega') \int_{t_0}^{t_0+\Delta t} p_{eq}(\Omega', t|\Omega_0, t_0)\, dt \right. \\ &\quad \left. - W(\Omega'|\Omega) \int_{t_0}^{t_0+\Delta t} p_{eq}(\Omega, t|\Omega_0, t_0)\, dt \right] d\Omega' \end{aligned} \tag{34}$$

note that $p_{eq}(\Omega,t_0|\Omega_0,t_0) = \delta(\Omega - \Omega_0)$ by the definition of a conditional probability. Further, we neglect all the terms

of order Δt^2 or higher, so the following integral is approximated as

$$\int_{t_0}^{t_0+\Delta t} p_{\mathrm{eq}}(\Omega, t|\Omega_0, t_0)\, \mathrm{d}t \cong \Delta t \delta(\Omega - \Omega_0) \tag{35}$$

Hence, integrating over Ω', eq 34 simplifies to

$$p_{\mathrm{eq}}(\Omega, t_0+\Delta t|\Omega_0, t_0) \cong W(\Omega|\Omega_0)\Delta t + \delta(\Omega - \Omega_0)\left[1 - \Delta t \int W(\Omega'|\Omega)\, \mathrm{d}\Omega'\right] \tag{36}$$

The left side is the probability of being in configuration Ω at time $t + \Delta t$, given conformation Ω at time t. The first term on the right side is the probability of changing conformation within Δt, the second term is the probability to stay in the same conformation. If we pick Δt such that the last term is zero

$$\Delta t = 1 \Big/ \int W(\Omega'|\Omega_0)\, \mathrm{d}\Omega' \tag{37}$$

then eq 36 becomes

$$p_{\mathrm{eq}}(\Omega, t_0+\Delta t|\Omega_0, t_0) \cong W(\Omega|\Omega_0)\Delta t \tag{38}$$

This means that within the specified time step the conformation Ω_0 must change by only one Kuhn step.

Using eq 5 and detailed balance, it is possible to calculate the transition probabilities for creation and destruction by SD for the last strand assuming a constant rate of destruction as done in eq 9

$$W^{\mathrm{SD}}_{\mathrm{d},Z-1}(\Omega'|\Omega) = \delta_{Z,Z'+1}\delta_{N_{Z-1},N'_{Z'}-1}\delta_{N_Z,1}\frac{2(\beta+1)}{\tau_{\mathrm{K}}(N_{Z-1}+1)}\prod_{j=1}^{Z-1}\delta_{\Omega_j,\Omega'_{j-1}}$$

$$W^{\mathrm{SD}}_{\mathrm{c},Z}(\Omega'|\Omega) = \delta_{Z,Z'-1}\delta_{N_Z,N'_{Z'-1}+1}H(N_Z-2)\frac{2(\beta+1)p^{\mathrm{CD}}(\tau_1^{\mathrm{CD}'})}{\tau_{\mathrm{K}}\beta N_Z} \times \left[\frac{3}{2\pi(N_Z-1)a_{\mathrm{K}}^2}\right]^{3/2}\exp\left[-\frac{3Q'^2_{Z-1}}{2(N_Z-1)a_{\mathrm{K}}^2}\right]\prod_{j=2}^{Z}\delta_{\Omega_j,\Omega'_{j+1}} \tag{39}$$

The transition probabilities for destruction and creation by CD for the last strand are

$$W^{\mathrm{CD}}_{\mathrm{d},Z-1}(\Omega'|\Omega) = \delta_{Z,Z'+1}\frac{1}{\tau^{\mathrm{CD}}_{z-1}}\prod_{j=1}^{Z-2}\delta_{\Omega_j,\Omega'_j}\delta(\boldsymbol{Q}'_{Z-1})\delta_{N_Z-1,N_Z,N'_{Z'-1}}$$

$$W^{\mathrm{CD}}_{\mathrm{c},Z}(\Omega'|\Omega) = \boldsymbol{\delta}_{Z,Z'-1}\frac{1}{\tau^{\mathrm{CD}}_{z-1}}\prod_{j=1}^{Z-1}\boldsymbol{\delta}_{\Omega_j,\Omega'_j}\boldsymbol{\delta}_{N_Z,N'_{Z'-1}+N'_{Z'}}H(N_Z-2) + N'_{Z+1}\frac{p^{\mathrm{CD}}(\tau_Z^{\mathrm{CD}'})}{\tau_Z^{\mathrm{CD}'}\beta}\times\left[\frac{3}{2\pi N'_{Z'-1}}\right]^{3/2}\exp\left[-\frac{3Q'^2_{Z'-1}}{2N'_{Z'-1}}\right] \tag{40}$$

Calculation of the Relaxation Modulus for a Rouse Chain with Random Mobilities. Rubinstein and Colby introduced the idea of using a Rouse chain with random mobilities to model constraint release of the tube. Likhtman and McLeish used the same idea, but with a modified distribution for the mobilities. Both groups used a distribution that was consistent with sliding dynamics, and both used a method from Dean. We used a method that is mathematically equivalent, but slightly different from the Dean technique, which yields the relaxation modulus for the Rouse chain, $R(t)$, plotted in Figure 19.

Consider a Rouse chain with $Z - 1$ entanglements, each has a mobility m_i drawn from a distribution given by the inverse Laplace transform of $\mu(t)$, as shown in reference.[3] The evolution equation for such a chain is

$$\frac{\partial p}{\partial t} = \sum_{i,j=1}^{Z-1}\overline{A}_{ij}\frac{\partial}{\partial \boldsymbol{Q}_i}\left[\frac{1}{k_{\mathrm{B}}T}\frac{\partial F}{\partial \boldsymbol{Q}_j}p + \frac{\partial p}{\partial \boldsymbol{Q}_j}\right] \tag{41}$$

where $\overline{A}_{ij}$ is an element of a modified Rouse matrix

$$\overline{A}_{ij} := \sum_{k=1}^{Z-1} m_k B_{ki} B_{kj} B_{ij} := \delta_{i,j-1} - \delta_{i,j} \tag{42}$$

Note that $\overline{A}$ is a tridiagonal matrix that couples neighboring strands. We can find the normal modes $\{\hat{\boldsymbol{Q}}_{\mathrm{i}}\}$ through a rotation matrix Ω_{ij}

$$\hat{A}_{km} := \sum_{i,j=1}^{Z-1}\Omega_{ik}\overline{A}_{ij}\Omega_{jm} \tag{43}$$

$$\hat{\boldsymbol{Q}}_i = \sum_{j=2}^{Z-1}\Omega_{ij}\boldsymbol{Q}_j \tag{44}$$

so that A is a diagonal matrix that consists of eigenvalues, $\hat{m}_i$, of the A matrix. It is straightforward to show that rotation of $\boldsymbol{Q}_i$ does not modify the form of the stress tensor (eq 23)

$$\tau = -\frac{3k_{\mathrm{B}}Tn}{N_e a_{\mathrm{K}}^2}\sum_{i=2}^{Z-1}\langle \boldsymbol{Q}_i\boldsymbol{Q}_i\rangle = -\frac{3k_{\mathrm{B}}Tn}{N_e a_{\mathrm{K}}^2}\sum_{j,k=2}^{Z-1}\sum_{i=2}^{Z-1}\Omega_{ij}\Omega_{ik}\langle \hat{\boldsymbol{Q}}_j\hat{\boldsymbol{Q}}_k\rangle \tag{45}$$

$$= -\frac{3k_{\mathrm{B}}Tn}{N_e a_{\mathrm{K}}^2}\sum_{j,k=2}^{Z-1}\delta_{j,k}\langle \hat{\boldsymbol{Q}}_j\hat{\boldsymbol{Q}}_k\rangle \tag{46}$$

$$= -\frac{3k_{\mathrm{B}}Tn}{N_e a_{\mathrm{K}}^2}\sum_{i=2}^{Z-1}\langle \hat{\boldsymbol{Q}}_i\hat{\boldsymbol{Q}}_i\rangle \tag{47}$$

The dimensionless relaxation modulus of the Rouse chain becomes

$$R(t) = \frac{1}{\langle Z\rangle_{\mathrm{eq}} - 1}\sum_{i=1}^{\langle Z\rangle_{\mathrm{eq}}-1}\langle \exp(-t\hat{m}_i)\rangle \tag{48}$$

Similar to the Dean method, we draw $\langle Z\rangle_{\mathrm{eq}} - 1$ mobilities from the distribution, construct the matrix $\overline{A}_{ij}$, and find its eigenvalues. On the order of 1000 such eigenvalues are found and used to estimate $R(t)$ through eq 48.

References and Notes

(1) Rubinstein, M.; Colby, R. H. *J. Chem. Phys.* **1988**, *89*, 5291–5306.
(2) Hua, C. C.; Schieber, J. D. *J. Chem. Phys.* **1998**, *109*, 10018–10027.
(3) Likhtman, A. E.; McLeish, T. C. B. *Macromolecules* **2002**, *35*, 6332–6343.
(4) de Gennes, P. G. *J. Phys.* (*Paris*) **1975**, *36*, 1199.
(5) Graessley, W. *Synth. Degrad. Rheol. Extrusion* **1982**, 67–117.
(6) Doi, M. *J. Polym. Sci., Polym. Lett. Ed* **1981**, *19*, 265.
(7) Doi, M.; Takimoto, J.-I. *R. Soc. London Philos. Trans., Ser. A* **2003**, *361*, 641–652.
(8) Nair, D. M.; Schieber, J. D. *Macromolecules* **2006**, *39*, 3386–3397.
(9) des Cloizeaux, J. *EPL* (*Europhys. Lett.*) **1988**, 437.
(10) Doi, M.; Edwards, S. *J. Chem. Soc. Faraday Trans. 2* **1978**, *74*, 1802–1817.
(11) Schieber, J. D.; Neergaard, J.; Gupta, S. *J. Rheol.* **2003**, *47*, 213–233.
(12) Schieber, J. D. *J. Chem. Phys.* **2003**, *118*, 5162–5166.
(13) Khaliullin, R. N.; Schieber, J. D. *Phys. Rev. Lett.* **2008**, *100*, 188302.
(14) Kampen, N. v. *Stochastic processes in physics and chemistry*; North-Holland: Amsterdam, 1992.
(15) Shlesinger, M. F.; Weiss, G. H. *The wonderful world of stochastics*; North Holland Physics Publishing: Amsterdam, 1985.
(16) Milner, S.; McLeish, T. *Macromolecules* **1997**, *30*, 2159–2166.
(17) Baumgaertel, M.; Schausberger, A.; Winter, H. H. *Rheol. Acta* **1990**, *29*, 400–408.
(18) Fetters, L.; Lohse, D.; Colby, R. *Phys. Prop. Polym. Handbook* **2007**, 447–454.
(19) Liu, C.-Y.; Halasa, A. F.; Keunings, R.; Bailly, C. *Macromolecules* **2006**, *39*, 7415–7424.
(20) Bach, A.; Almdal, K.; Rasmussen, H. K.; Hassager, O. *Macromolecules* **2003**, *36*, 5174–5179.
(21) Nair, R. R. M.Sc. Thesis, Illinois Institute of Technology: Chicago, IL, **2004**.
(22) Schweizer, T.; van Meerveld, J.; Ottinger, H. C. *J. Rheol.* **2004**, *48*, 1345–1363.
(23) van Ruymbeke, E.; Keunings, R.; Stephenne, V.; Hagenaars, A.; Bailly, C. *Macromolecules* **2002**, *35*, 2689–2699.
(24) Montfort, J. P.; Marin, G.; Arman, J.; Monge, P. *Rheol. Acta* **1979**, *18*, 623–628.
(25) Nielsen, J. K.; Rasmussen, H. K.; Hassager, O.; McKinley, G. H. *J. Rheol.* **2006**, *50*, 453–476.
(26) Watanabe, H.; Kotaka, T. *Macromolecules* **1984**, *17*, 2316–2325.
(27) Maier, D.; Eckstein, A.; Friedrich, C.; Honerkamp, J. *J. Rheol.* **1998**, *42*, 1153–1173.
(28) Baumgaertel, M.; Rosa, M. E.; Machado, J.; Masse, M.; Winter, H. H. *Rheol. Acta* **1992**, *31*, 75–82.
(29) Onogi, S.; Masuda, T.; Kitagawa, K. *Macromolecules* **1970**, *3*, 109–116.
(30) Liu; He; Keunings, R.; Bailly, C. *Macromolecules* **2006**, *39*, 3093–3097.
(31) Masubuchi, Y.; Watanabe, H.; Ianniruberto, G.; Greco, F.; Marrucci, G. *Macromolecules* **2008**, *41*, 8275–8280.
(32) Schieber, J. D. *J. Non-Equilibr. Thermodyn.* **2003**, *28*, 179–188.
(33) Neergaard, J.; Schieber, J. D. *XIIIth International Congress on Rheology*; Binding, D. M., Hudson, N. E., Mewis, J., Piau, J.-M., Petrie, C. J. S., Townsend, P., Wagner, M. H., Walters, K., Eds.; British Society of Rheology: 2000; pp 120−122.
(34) Likhtman, A. E. *Macromolecules* **2005**, *38*, 6128.
(35) Ramírez, J.; Sukumaran, S. K.; Likhtman, A. E. *Macromol. Symp.* **2007**, *252*, 119–129.
(36) Watanabe, H.; Matsumiya, Y.; Inoue, T. *Macromol. Symp.* **2005**, *228*, 51–70.
(37) Watanabe, H. *Macromol. Rapid Commun.* **2001**, *22*, 127–175.
(38) Milner, S. T.; McLeish, T. C. B. *Phys. Rev. Lett.* **1998**, *81*, 725–728.
(39) Auhl, D.; Ramirez, J.; Likhtman, A. E.; Chambon, P.; Fernyhough, C. *J. Rheol.* **2008**, *52*, 801–835.